Environmental Science & Technology

pubs.acs.org/est

Article

Selectivity in Enzymatic Phosphorus Recycling from Biopolymers: Isotope Effect, Reactivity Kinetics, and Molecular Docking with Fungal and Plant Phosphatases

Mina Solhtalab, Spencer R. Moller, April Z. Gu, Deb Jaisi, and Ludmilla Aristilde*

Cite This: *Environ. Sci. Technol.* 2022, 56, 16441−16452

Read Online

ACCESS | Metrics & More | Article Recommendations | Supporting Information

ABSTRACT: Among ubiquitous phosphorus (P) reserves in environmental matrices are ribonucleic acid (RNA) and polyphosphate (polyP), which are, respectively, organic and inorganic P-containing biopolymers. Relevant to P recycling from these biopolymers, much remains unknown about the kinetics and mechanisms of different acid phosphatases (APs) secreted by plants and soil microorganisms. Here we investigated RNA and polyP dephosphorylation by two common APs, a plant purple AP (PAP) from sweet potato and a fungal phytase from *Aspergillus niger*. Trends of $\delta^{18}O$ values in released orthophosphate during each enzyme-catalyzed reaction in ^{18}O-water implied a different extent of reactivity. Subsequent enzyme kinetics experiments revealed that *A. niger* phytase had 10-fold higher maximum rate for polyP dephosphorylation than the sweet potato PAP, whereas the sweet potato PAP dephosphorylated RNA at a 6-fold faster rate than *A. niger* phytase. Both enzymes had up to 3 orders of magnitude lower reactivity for RNA than for polyP. We determined a combined phosphodiesterase-monoesterase mechanism for RNA and terminal phosphatase mechanism for polyP using high-resolution mass spectrometry and ^{31}P nuclear magnetic resonance, respectively. Molecular modeling with eight plant and fungal AP structures predicted substrate binding interactions consistent with the relative reactivity kinetics. Our findings implied a hierarchy in enzymatic P recycling from P-polymers by phosphatases from different biological origins, thereby influencing the relatively longer residence time of RNA versus polyP in environmental matrices. This research further sheds light on engineering strategies to enhance enzymatic recycling of biopolymer-derived P, in addition to advancing environmental predictions of this P recycling by plants and microorganisms.

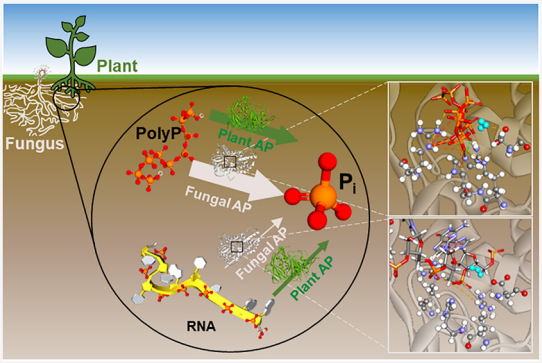

KEYWORDS: *phytase, purple acid phosphatase, plant, fungi, phosphorus recycling, polyphosphate, ribonucleic acid, molecular docking simulations, liquid chromatography−mass spectrometry, nuclear magnetic resonance, oxygen isotope, phosphorus mineralization*

1. INTRODUCTION

Phosphorus-containing biopolymers (P-biopolymers) represent slow-releasing phosphorus (P) reservoirs for plants and soil microorganisms,[1−4] especially in the upper horizon of young soils.[5] With dependence on the land usage, soils can contain a range of concentrations of P-biopolymers, including ribonucleic acids (RNAs) (1−56 mg RNA-P kg^{-1} soil) and inorganic polyphosphates (polyPs) (5−50 mg P kg^{-1} soil).[5−7] In agricultural soils, fertilizer application can result in elevated levels of P-biopolymers.[5,8] Intracellularly, there are enzymes that specifically hydrolyze polyP and RNA.[9−11] For polyP, intracellular exo- and endopolyphosphatases cleave phosphoanhydride bonds from the end or the middle of the polyP chains, respectively;[11] for RNA, intracellular phospho-diesterases (P-diesterases) such as ribonucleases produce ribonucleotides, which are subsequently hydrolyzed by phospho-monoesterases (P-monoesterases) to ribonucleosides and orthophosphate (inorganic P or P_i).[10,12] Compared to the aforementioned intracellular enzymes, extracellular P-monoesterases have higher stability in the soil environment and are found at up to 2-fold higher abundance.[13−15] Furthermore, extracellular P-monoesterases, which include acid phosphatases (APs) and phytases, are reportedly in excess in soils because their activity is limited by the concentrations of phosphomonoester (P-monoester) substrates.[13] Notably, compared to carbon recycling enzymes (e.g., β-glucosidases, cellobiosidases, xylosidases) involved in the breakage of glycosidic bonds, two to three times higher activity was found for P-monoesterases in soil.[16] Despite the ubiquitous secretion of P-monoesterases by plants and soil microorganisms, much remains unknown about

Received: July 11, 2022
Revised: October 5, 2022
Accepted: October 5, 2022
Published: October 25, 2022

the potential catalytic role of these enzymes in recycling P_i from P-biopolymers.

We focus here on the reactivity of APs, which represent a subset of P-monoesterases secreted by plant roots and microbes and are widely implicated in recycling P_i from organic compounds in soils.[16−21] With the use of 4-nitrophenyl phosphate as a model synthetic substrate, a six-to-ten times higher activity was observed from APs compared to alkaline phosphatases in soil.[22] Two common types of APs are purple APs (PAPs) secreted by plants and phytases secreted by fungi. Up-regulation of gene expressions of both PAPs and phytases has been reported in soils with P_i deficiency.[16,23] The plant PAPs are binuclear metallohydrolases that can dephosphorylate a wide range of P-monoester substrates including ribonucleotides, phytic acid, and phosphoenolpyruvate.[23] Phytases specifically target monoester bonds in inositol hexakis-phosphate or phytate,[24] but some phytases including those from the fungi *Aspergillus niger* and *Peniophora lycii* also exhibit reactivity toward a diverse range of organic substrates, including sugar phosphates and multiphosphorylated ribonucleotides.[25,26] Interestingly, phytase from *A. niger* is widely reported to be abundant in the soil environment.[22,27] Previous studies have reported polyP hydrolysis by plant APs from wheat (*Triticum aestivum*) and sweet potato (*Ipomoea batatas*), phytase from the fungus *Aspergillus niger*, alkaline phosphatase from *Escherichia coli*, and pyrophosphatase from the yeast *Saccharomyces cerevisiae*.[28,29] Regarding the relative hydrolysis of P-biopolymers catalyzed by APs of different biological origins, the relative kinetic parameters and the mechanisms of substrate specificity remain to be elucidated.

Here we sought to investigate the catalytic reactivity and substrate binding mechanisms for the dephosphorylation of polyP and RNA by representative extracellular APs of plant and fungal sources, respectively, plant PAPs and fungal phytases and APs (Figure 1A). We performed dephosphorylation kinetic experiments and ^{18}O-isotope tracing of released P_i with *A. niger* phytase and sweet potato PAP. We determined the mechanisms of the hydrolytic cleavage by monitoring the products of polyP hydrolysis by ^{31}P nuclear magnetic resonance spectroscopy (^{31}P NMR) and the products of RNA hydrolysis by high-resolution liquid chromatography−mass spectrometry (LC−MS). To obtain mechanistic insights, we conducted docking simulations of polyP or RNA with model structures of four plant PAPs [from sweet potato (*Ipomea batatas*), red kidney bean (*Phaseolus vulgaris*), wheat (*Triticum aestivum*), and thale cress (*Arabidopsis thaliana*)] and four fungal phytases or APs (from *A. niger*, *Debaryomyces castellii*, *Kluyveromyces lactis*, and *S. cerevisiae*). The findings from this research provide new insights into the mechanistic basis for the potential recycling (or lackthereof) from P-biopolymers catalyzed by common APs secreted by plants and fungi. Such insights are critical to evaluating different biological processes in natural P recycling and inform the design of sustainable P-management strategies.

2. MATERIALS AND METHODS

2.1. Chemicals. Sodium glass phosphate type 45 (polyP-45, S4379), ribonucleic acid type VI from *Cyberlindnera jadinii* (torula yeast) (R6625), and PAP from *Ipomea batatas* (sweet potato) (P1435) were purchased from Sigma. PolyP-130 was synthesized as described previously.[30] Fungal phytase from *A. niger* (Natuphos) was a gift from BASF company (NJ, USA). Details on the sources of other chemicals used in this study are provided in the Supporting Information, Appendix A. The details on the enzyme purification and RNA characterization are described in Supporting Information, Appendices B and C.

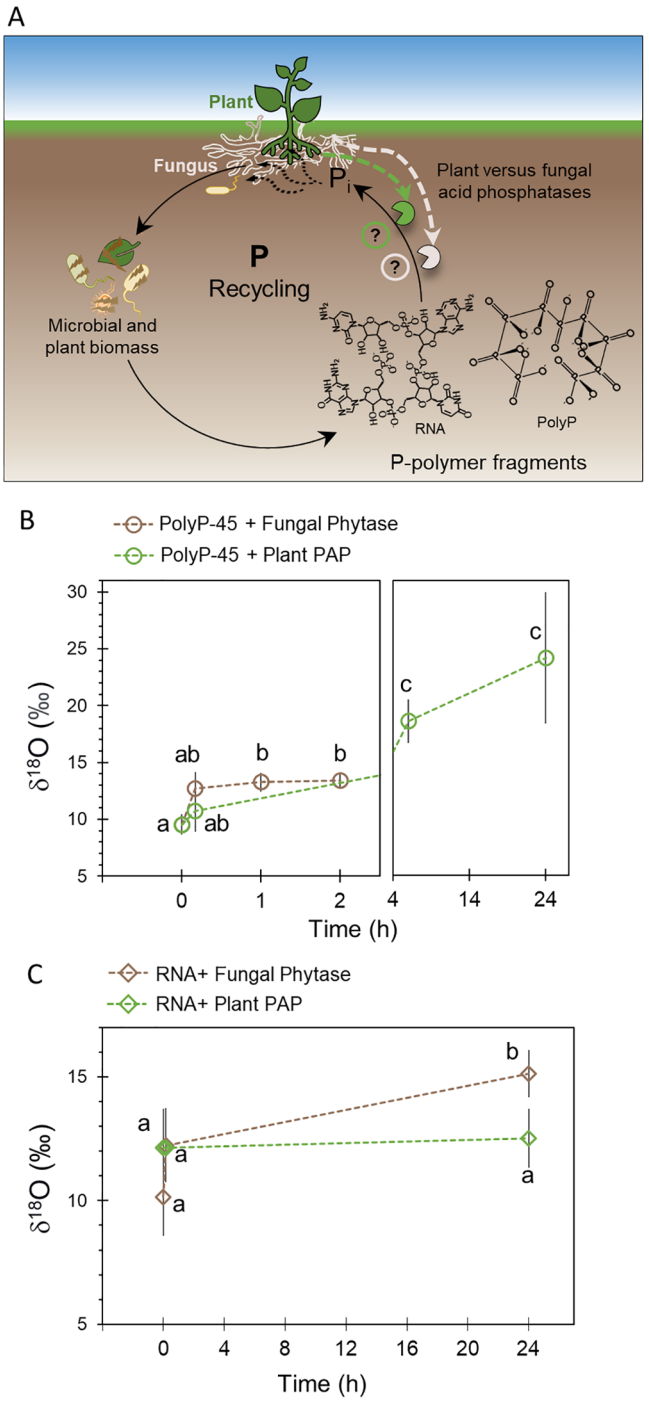

Figure 1. (A) Schematic overview of P recycling from selected P-biopolymers (RNA and polyp) in soil and the potential role of plant and microbial acid phosphatases. Time-dependent $\delta^{18}O$ of P_i during the dephosphorylation reactions of (B) polyP-45 and (C) RNA catalyzed by a fungal phytase from *A. niger* (brown symbols) and PAP from sweet potato (green symbols). Error bars indicate the standard deviation around the mean (n = 3). Data with statistically significant differences (P > 0.05) are indicated with different letters. The lines connecting the data points in panels (A) and (B) are meant as guides to the eye and do not reflect linear trends of the data.

https://doi.org/10.1021/acs.est.2c04948
Environ. Sci. Technol. 2022, 56, 16441−16452

2.2. Measurement of Oxygen Isotope Values. Substrate solutions were made with 0.1 M sodium acetate buffer prepared using ^{18}O-enriched water (with $\delta^{18}O_W$ value of 27 ‰). We reacted 3.6 mU (0.36 μg) of *A. niger* phytase or 36 mU (0.84 μg) sweet potato PAP in 100 mL polyP-45 solution (100 μM polyP chains) and 360 mU (36 μg) *A. niger* phytase or 120 mU (2.76 μg) sweet potato PAP in 100 mL RNA solution (3.3 g L^{-1}). Replicate reactions were run at optimal conditions for each enzyme: pH 5 and 25 °C for sweet potato PAP[31] and pH 5.3 and 37 °C for *A. niger* phytase (according to the manufacturer; BASF, NJ, USA). At specific time points (10 min; 1, 2, 6, or 24 h), the reaction was stopped by immersing an aliquot in liquid nitrogen followed by sample storage at −20 °C until the time of analysis. The oxygen isotope values in P_i ($\delta^{18}O_P$) were measured in silver phosphate analyte, which was prepared after a multistep purification process that included removing contaminants and enriching P_i following previously published methods.[32,33] A detailed protocol is provided in Supporting Information, Appendix D.

2.3. Kinetics of polyP or RNA Dephosphorylation by the Plant and Fungal APs. We reacted 0.036 mU of each enzyme (3.6 ng) of *A. niger* phytase by adding 10 μL from a stock or (0.84 ng of sweet potato PAP by adding 1 μL from a stock) in 100 mL substrate solution containing different concentrations of polyP-45 or polyP-130 (1, 5, 10, 20, 40, and 60 μM polyP chains), or RNA (0.33, 1.7, 3.3. 6.7, and 10 g L^{-1}). Reactions were run in triplicates at the aforementioned optimum conditions (see the previous section) for each enzyme. For polyP kinetics, the reaction solutions were immediately assayed for P_i at specific time points using the ammonium molybdate method.[34] Due to precipitation of molybdate in RNA solutions, this method could not be used to monitor P_i during RNA dephosphorylation. Therefore, we employed a high-resolution LC−MS-based metabolomics method[35] to monitor the concentration of ribonucleotides (adenosine monophosphate, AMP; guanosine monophosphate, GMP; cytidine monophosphate, CMP; uridine monophosphate, UMP), ribonucleosides (adenosine, guanosine, cytidine, and uridine), and nucleobases (adenine, guanine, cytosine, and uracil). To stop the RNA dephosphorylation reactions at specific time points, 3 mL aliquots were immersed in liquid nitrogen, and the samples were stored at −20 °C until the time of analysis. The amount of released P_i was calculated based on the increase in the concentration of ribonucleosides in the solution. The half saturation constants (k_m) and maximum rates (V_{max}) of the fungal phytase or the plant PAP for polyP and RNA dephosphorylation were calculated by fitting a Michaelis−Menten curve over the experimental data points using a Microsoft Excel Solver tool.

2.4. Monitoring the polyP Hydrolysis Products Using ^{31}P NMR. To probe the mechanisms of polyP hydrolysis, we used a higher concentration of polyP-45 than the above kinetics experiments to obtain measurable signals with ^{31}P NMR. These polyP dephosphorylation reactions (pH 5) were run by reacting 3.6 ng of *A. niger* phytase or sweet potato PAP in 1 mL polyP-45 solution (with 2 mM polyP chains) at the aforementioned optimal conditions for each enzyme. At specific time points (10 min, 2 h, and 24 h), deuterium oxide (10% v/v) was added to each sample before immediate analysis of the hydrolysis products by ^{31}P NMR (Bruker Avance III HD system equipped with a BBO Prodigy probe) at the Integrated Molecular Structure Education and Research Center (IMSERC) at Northwestern University (Evanston, IL). For each sample, 32 scans were obtained with a 0.4 s acquisition time and 2.0 s pulse delay. We tracked chemical shifts at −10, −21, and 0.1 ppm for terminal phosphate moieties, the middle phosphate moieties, and the P_i, respectively. The peak positions in the NMR spectra were found to be stable and did not change during the course of the reaction. Therefore, besides automatic baseline correction, no further correction was applied to the NMR spectra.

2.5. Molecular Docking Simulations with Molecular Dynamics Equilibration. To consider the relevance of our experimental results with respect to diverse structures of APs, we conducted molecular simulations with four different plant PAPs and four different fungal APs, exhibiting a range of substrate specificities. Tertiary (3D) structures of the following enzymes were obtained from the protein data bank (PDB): phytase A from *A. niger* (PDB ID 3K4Q), phytase from *D. castellii* (PDB ID 2GFI), PAP from sweet potato (*I. batatas*; PDB ID 1XZW), PAP from red kidney bean, (*P. vulgaris*; PDB ID 6PY9), and PAP from wheat (*T. aestivum*; PDB ID 6GJ2). Additionally, the coordinates for the 3D structures of the PAP type 15 from thale cress (*A. thaliana*) and the fungal APs from *K. lactis* (PHO5) and *S. cerevisiae* (PHO11) were obtained from the available Swiss models with the best qualitative model energy analysis scores.[36] With the use of Discovery Studio software,[37] water molecules and heteroatoms, except the catalytic metal ions, were removed from the protein structures and hydrogen atoms were added. Next, geometry optimization was performed to fix any possible clashes from the structures. To prepare the metalloenzymes (*i.e.*, the plant PAPs), the positions of their specific metal cations (Fe^{2+}, Fe^{3+}, Mn^{2+}, or Zn^{2+}) and their coordinating amino acid residues were fixed. All enzyme structures were prepared at pH 5 by manually setting the prominent protonation states of amino acid residues at this pH. For the docking simulations with polyP, we used the 3D structure of polyP-9 from a crystal structure of polyphosphate kinase (PDB ID 5LL0)[38] and subsequently prepared it at pH 5. Here, we focused specifically on the orientation of the scissile bond in the terminal phosphate in the active site. In this case, the size of the substrate does not determine the binding parameters investigated. For the docking simulations with polyP and RNA, a polyP-9 chain or a sequence of ribonucleotides (AGCUACUCG) was introduced as the ligand, respectively. The docking of polyP-9 and RNA into the active site of each enzyme was performed using the CDOCKER protocol in Discovery Studio[37] and the HDOCK server,[39] respectively. Each enzyme structure was used as the receptor, and the catalytic residues were assigned as the receptor binding sites. Among the top ten hits of the docked substrate from CDOCKER or HDOCKER, we selected one for further simulations based on the orientation of the substrate, the number of interactions with catalytic residues, and the docking scores, the latter of which accounted for the internal ligand strain energy and the receptor−ligand interaction energy. The substrate-enzyme complexes were then subjected to 2000 steps of energy minimization, followed by solvation in a water box with ionic strength of 0.145 M provided by Na^+ and Cl^- ions. The hydrated energy-minimized systems were subjected to a 10 ns molecular dynamics equilibration, using the CHARMM force field and TIP3P water model for partial charge assignments for the enzyme and water atoms, respectively. The ligand-interaction protocol and trajectory analysis tool in Discovery Studio were used to evaluate the hydrogen (H) bonding, electrostatic interactions,

https://doi.org/10.1021/acs.est.2c04948
Environ. Sci. Technol. 2022, 56, 16441−16452

and distances between the substrate and specific amino acid residues in the active site of each enzyme.

2.6. Statistical Analysis. Significant differences between experimental data, set at $P < 0.05$, were determined by performing unpaired t tests between two sets of data using GraphPad Prism (9.3.1).

3. RESULTS AND DISCUSSION

3.1. Trend in $\delta^{18}O_p$ Values Implies Enzyme-Dependent Dephosphorylation of Each P-biopolymer. Change in $\delta^{18}O$ associated with P_i has been used previously to investigate the involvement of different biological P recycling processes in natural soils and agroecosystem environments.[29,40−43] Different profiles of isotopic exchange were monitored previously during the dephosphorylation of different substrates including phytate, glycerophosphate, and a ribonucleotide catalyzed by *A. niger* phytase and a wheat AP.[41,44] In these previous studies,[41,44] the oxygen isotope fractionations were found to be different for the hydrolysis of the same substrates catalyzed by both enzymes, thus suggesting different catalytic mechanisms for these enzymes. Here, to obtain preliminary insights on the different reactivity of *A. niger* phytase and sweet potato PAP, we tracked the $\delta^{18}O_P$ of the released P_i as a function of reaction time with polyP and RNA in solution with ^{18}O-water (Figure 1B,C).

We obtained distinct $\delta^{18}O_P$ values during polyP and RNA reactions with each enzyme. First, there was minimal change in the $\delta^{18}O_P$ values (only up to 5% difference at a 24 h reaction time compared to a 10 min reaction time) during the *A. niger* phytase reaction with polyP and the sweet potato PAP reaction with RNA, averaging at 12.23 (±0.74) ‰ and 11.60 (±0.96) ‰, respectively (Figure 1B,C). These results are consistent with a reported near-constant isotope value during hydrolysis reactions of phytate by *A. niger* phytase by Sun et al.[44] On the other hand, the $\delta^{18}O_P$ values during the *A. niger* phytase reaction with RNA and the sweet potato PAP reaction with polyP were appreciably increased, specifically to 15.13 (±0.58) ‰ and 24.17 (±1.01) ‰ after 24 h, respectively (Figure 1B,C). These changes in $\delta^{18}O_P$ values, corresponding between 24% to 2-fold increase relative to the values at the start of the reaction, indicated a Rayleigh type fractionation during RNA reaction with *A. niger* phytase and the polyP reaction with sweet potato PAP (Figure 1B,C). The association of the released P_i to a Rayleigh type fractionation[45] was due to isotopic enrichment occurring as a function of reaction time, as reported commonly in carbonate and organic compound hydrolysis.[46−49]

For each investigated P-polymer (polyP versus RNA), we posit that the observed increase in $\delta^{18}O_P$ values with one enzyme, compared to no change in $\delta^{18}O_P$ values with another enzyme, was indicative of slower reactivity kinetics of one enzyme relative to the other (Figure 1B,C). Therefore, our $\delta^{18}O_P$ data implied a preference of the fungal enzyme over the plant PAP for polyP and a preference of the plant PAP over the fungal phytase for RNA. To obtain corroborative insights on this proposed substrate-dependent enzyme reactivity, we conducted kinetic reactions with different concentrations of polyP and RNA to determine the enzyme kinetics parameters (Figure 2).

3.2. Fungal Phytase Dephosphorylates polyP Faster than Plant PAP. We conducted experiments with two polyP chains containing different amounts of phosphates, polyP-45 and polyP-130, to examine the influence of the polyP chain

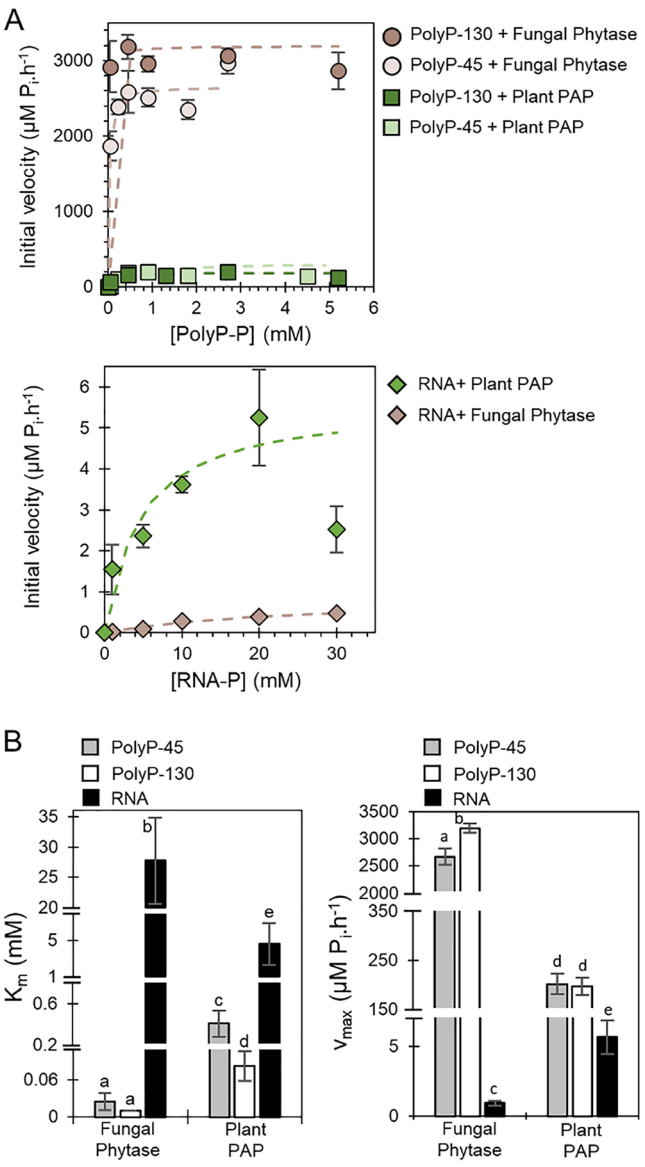

Figure 2. (A) Kinetics data of (top) polyP and (bottom) RNA dephosphorylation by a fungal phytase (from *A. niger*, brown symbols) and a plant PAP (from sweet potato, green symbols) as a function of substrate concentrations shown as P-equivalent concentrations; the dashed lines represent Michaelis−Menten curves using parameters determined with the data. (B) Calculated values of (left) half-saturation constants (K_m) and (right) maximum rates (V_{max}) for the dephosphorylation of polyP-45 (gray bars), polyP-130 (white bars), and RNA (black bars) catalyzed by the fungal phytase and the plant PAP. Error bars represent the standard deviation around the mean ($n = 3$). Statistically significant differences ($P < 0.05$) in panel (B) are indicated by different letters.

length on enzyme activity (Figure 2A). The *A. niger* phytase reached its V_{max} (on average, 2649 μM P_i h^{-1} for polyP-45 and 2863 μM P_i h^{-1} for polyP-130) at a low concentration for both polyP chains, reflecting its high affinity with a low K_m value (10−20 μM P) (Figure 2A,B). While the V_{max} of *A. niger* phytase was 20% higher for polyP-130 than polyP-45 ($P < 0.05$), the K_m values were not statistically significant ($P = 0.12$) (Figure 2B). By contrast, sweet potato PAP reached a similar V_{max} of about 200 μM P_i h^{-1} for both polyP chains but had a significantly higher affinity for polyP-130 ($K_m \sim 0.08$ mM-P) than polyP-45 ($K_m \sim 0.41$ mM-P) ($P < 0.05$) (Figure 2B).

https://doi.org/10.1021/acs.est.2c04948
Environ. Sci. Technol. 2022, 56, 16441−16452

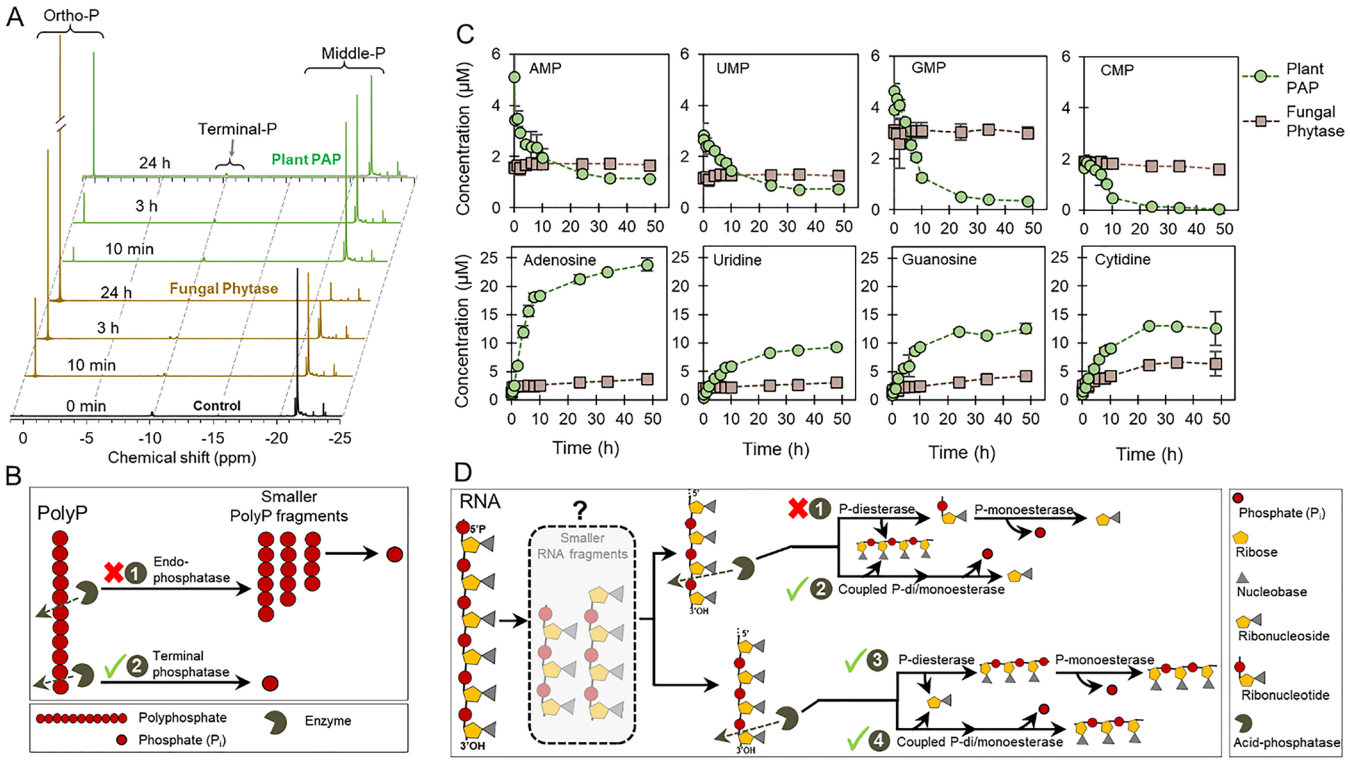

Figure 3. (A) Time-dependent ^{31}P NMR spectra of polyP-45 dephosphorylation by fungal phytase (from *A. niger*, brown spectra) and plant PAP (green spectra); the reference spectrum of polyP-45 in solution (control) is shown in black at the bottom. Indicated in the spectra are the peaks related to the orthophosphate (Ortho-P), terminal phosphate in the polyP chain (Terminal-P), and middle phosphate in the polyP chain (Middle-P). (B) Schematic representation of two proposed phosphatase mechanisms, endo versus terminal cleavage of the polyP chain, during polyP dephosphorylation; the ^{31}P NMR data support the terminal phosphatase mechanism (indicated by the green check) and do not support an endophosphatase reaction (indicated by the red cross). (C) Time-dependent changes in the LC−MS-measured concentrations of ribonucleotides (top row) and ribonucleosides (bottom row) during RNA dephosphorylation reactions catalyzed by the fungal phytase (brown) and plant PAP (green) at a concentration of 10 mM RNA-P; measured ribonucleotide impurities ranged between 8 and 14 μM. Error bars represent the standard deviation around the mean (n = 3). (D) Schematic illustration of four proposed mechanisms for enzymatic RNA cleavage; the possible production of short RNA fragments due to an endonuclease activity (indicated with a question mark) could not be resolved by our data. The data do not support Mechanism 1 (indicated with a red ×), which would generate ribonucleotides. The data are consistent with the mechanisms wherein ribonucleosides are released in the first step (mechanisms 2, 3, 4; indicated with a green check mark).

Therefore, the V_{max} for polyP hydrolysis was 10 to 20 times higher with the fungal phytase (*A. niger*) than with the plant PAP ($P < 0.05$) (Figure 2A). The low V_{max} values with sweet potato PAP could be due to the inhibition of enzyme activity by P_i at concentrations above 0.3 mM, as previously reported by Schenk *et al.*[31] In sum, the enzyme kinetic parameters obtained with RNA indicated greater reactivity of sweet potato PAP than *A. niger* phytase, in agreement with the differences in the isotope effects, we obtained during the enzymatic reactions with RNA.

3.3. Slow Dephosphorylation of RNA by the Plant and Fungal APs. We found that both sweet potato PAP and *A. niger* phytase can dephosphorylate RNA but at 2 and 3 orders of magnitude slower rates, respectively, compared to polyP ($P < 0.05$) (Figure 2A,B). Notably, the V_{max} of RNA dephosphorylation was 0.92 μM P_i h^{-1} (on average) with *A. niger* phytase, which was about 5 times lower than the V_{max} with sweet potato PAP (5.62 μM P_i h^{-1}, on average) ($P < 0.05$) (Figure 2B). Interestingly, the RNA hydrolysis rates with the sweet potato PAP decreased to 2.52 μM P_i h^{-1} at RNA-P above 20 mM after reaching its maximum value (Figure 2A), suggesting an RNA concentration threshold at which substrate inhibition occurred with the plant PAP. This decreasing trend was not observed with *A. niger* phytase (Figure 2A).

3.4. Terminal-Phosphatase Mechanism for Enzymatic polyP Dephosphorylation. Using ^{31}P NMR, we elucidated the enzymatic mechanism of polyP hydrolysis by monitoring the distinctive chemical shifts in the NMR spectra (Figure 3A,B).[28,50] The terminal phosphate moieties (terminal-P) and the middle phosphate moieties (middle-P) have peaks at −10 and −21 ppm, respectively; the free orthophosphate (or P_i) has a peak around 0.1 ppm (Figure 3A).[50] We evaluated two possible mechanisms for the hydrolytic cleavage of the polyP molecule (polyP-45). For mechanism 1, we considered an endophosphatase mechanism wherein the phospho-anhydride bonds (P−O−P) would be cleaved from the middle of the chain to produce shorter fragments of polyP (Figure 3B). Such increase in the amount of short polyP fragments would increase the peak intensities for the terminal-P signal but decrease the peak intensity for middle-P.[28] For mechanism 2, we considered a terminal phosphatase mechanism, in which a phosphate moiety in the polyP would be cleaved one after the other from either end of the polyP chain (Figure 3B). With this latter mechanism, the peak intensity of the terminal-P signal would remain unchanged, but the peak intensity for the middle-P would decrease due to shortening of the polyP chains.[28]

https://doi.org/10.1021/acs.est.2c04948
Environ. Sci. Technol. 2022, 56, 16441−16452

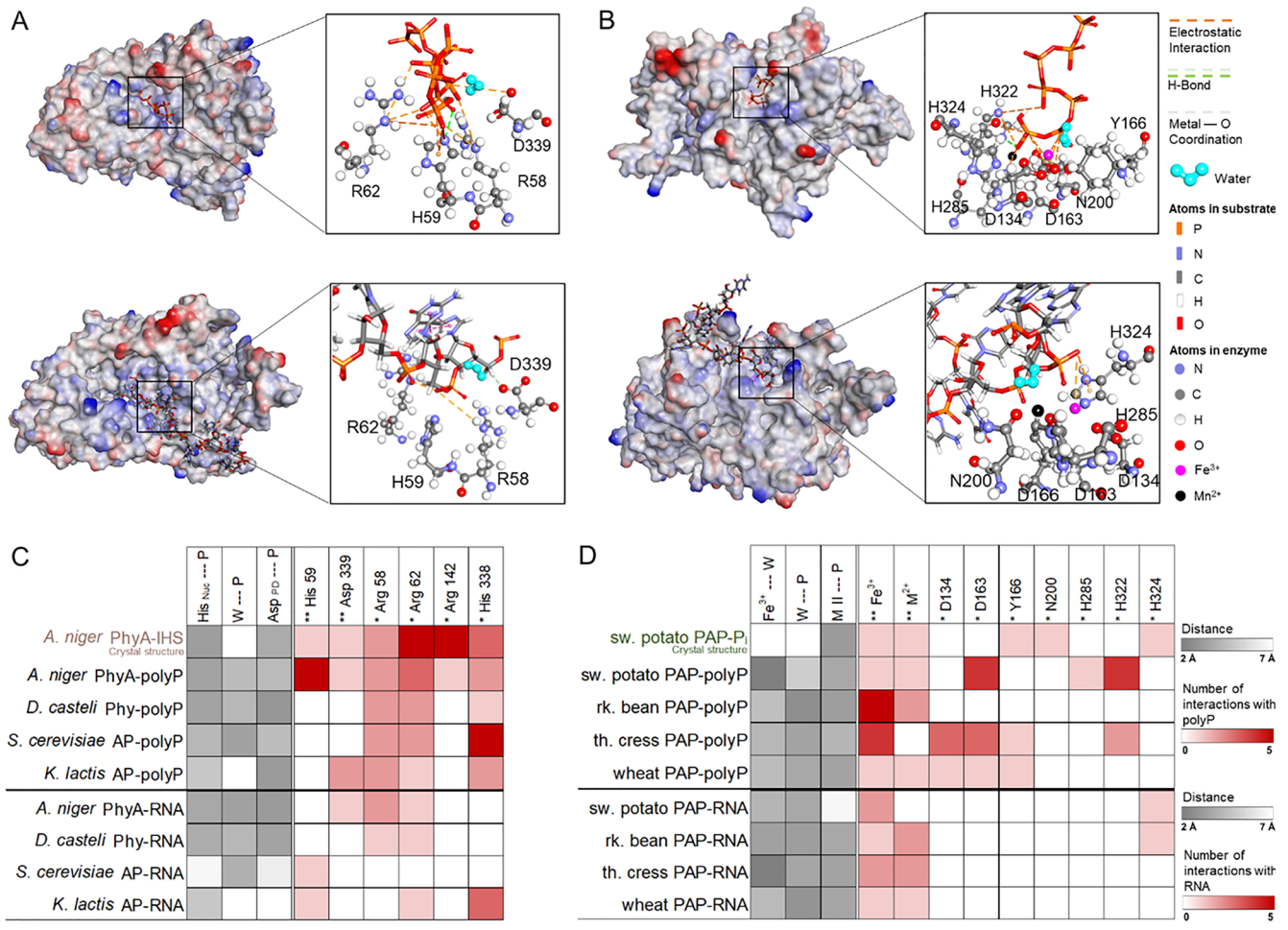

Figure 4. Molecular dynamics-equilibrated complexes of (A) a fungal phytase (from *A. niger*) and (B) a plant PAP (from sweet potato) with polyP-9 (top) and RNA (bottom). The enzyme surfaces (left in each panel) are color-coded according to their interpolated charges (blue/red = positive/negative), and the close-up panels (right) show the interactions of the substrate with water, metal cations, and amino acid residues in the active site. Heat maps of interactions of polyP and RNA in the substrate binding pocket of (C) fungal phytases and APs and (D) plant PAPs. The gray heat maps present three important distances in the precatalytic substrate-enzyme complexes in comparison to the corresponding distances in the reference crystal structures (first row in C and D). In the fungal phytases and APs (C), these precatalytic distances include the distance between the nucleophile histidine (His_{Nuc}---P), or a water molecule (W---P), or the proton-donor aspartate (Asp_{PD}---P) and the target phosphate moiety in the substrate. In the plant PAPs (D), these precatalytic distances include the distance between Fe^{3+} and a water molecule (Fe^{3+}---W), the distance between the target phosphate moiety in the substrate and the water molecule (P---W) or the divalent metal cation (P---M^{2+}; M^{2+} is Mn^{2+} in sweet potato PAP, Zn^{2+} in red kidney bean PAP, Fe^{2+} in thale cress PAP, and Fe^{2+} in wheat PAP). The red heat maps present the number of active site interactions with polyP (shown above the black line) or RNA (shown below the black line in the table) in (C) the fungal APs and (D) plant APs. The catalytic amino acid residues (labeled with **) and other active site amino acid residues (labeled with *) in fungal APs (C) are numbered based on the reference structure of *A. niger* phytase and in plant PAPs (D) based on the reference structure of sweet potato PAP. The corresponding residue numbers in other phytases and PAPs are listed in the Supporting Information, Appendix G.

In the ^{31}P NMR spectra of the polyP-45 control sample, there was an intense peak for the middle-P (at −10.23 ppm), whereas relatively minor to non-noticeable peaks for both the terminal-P and P_i were detected, consistent with high abundance of polyP chains in the starting polyP solution (Figure 3A). During the 24 h reaction time, the polyP hydrolysis by sweet potato PAP led to a gradual decrease in the peak intensity of middle-P (up to −40%) accompanied by a greater than 300-fold increase in the peak intensity for P_i, but the peak intensity for the terminal-P remained unchanged (Figure 3A and Supporting Information, Appendix E). In a similar fashion, there was no increase in the peak intensity of the terminal-P during the polyP hydrolysis by *A. niger* phytase, but there was a 300-fold decrease in the intensity of the middle-P peak and a near 700-fold increase in the P_i peak intensity (Figure 3A and Supporting Information, Appendix E). The relatively higher peak intensities with *A. niger* phytase compared with sweet potato PAP are consistent with the aforementioned enzyme kinetic parameters with polyP (Figures 2B and 3A). In sum, the time-dependent ^{31}P NMR data provided evidence of a terminal phosphatase mechanism for the polyP dephosphorylation by both plant and fungal APs, as characterized by a relative decrease in the middle-P signal combined with a significant increase in the P_i signal and no change in the minor terminal P signal (Figure 3B).

3.5. Evidence of Coupled P-diesterase and P-monoesterase Activity During RNA Dephosphorylation.

We evaluated four possible mechanisms for RNA dephosphorylation by *A. niger* phytase and sweet potato PAP by using LC−MS to monitor the RNA reaction products (Figure 3C,D). Upon hydrolysis of a P-diester bond, a P-monoester would be produced in the active site, which might be a

https://doi.org/10.1021/acs.est.2c04948
Environ. Sci. Technol. 2022, 56, 16441−16452

ribonucleotide or a shortened RNA fragment with a terminal-P, depending on the site of enzymatic cleavage (Figure 3D). For mechanisms 1 and 2, we considered cleavage at a terminal 3′O−P bond of RNA wherein the P-monoester product would be a ribonucleotide (Figure 3D). For mechanism 1, the ribonucleotide product generated through a P-diesterase reaction would be released in solution prior to the dephosphorylation by a subsequent P-monoesterase reaction (Figure 3D). For mechanism 2, the ribonucleotide would remain in the active site to undergo dephosphorylation immediately via a coupled P-diesterase/P-monoesterase mechanism (Figure 3D). For mechanisms 3 and 4, we considered the bond between O_P and the 5′C of a terminal nucleotide to be cleaved to produce a ribonucleoside and a shorter RNA fragment with a terminal phosphate (Figure 3D). For mechanism 3, the RNA fragment with 3′-P would be released from the active site before getting dephosphorylated in a separated step, whereas in mechanism 4, the RNA fragment would stay in the active site and get dephosphorylated immediately in a coupled P-diesterase/monoesterase mechanism similar to mechanism 2 (Figure 3D). After the first step of the catalysis in the latter three mechanisms (mechanisms 2, 3, and 4), a ribonucleoside would be released, but a ribonucleotide would be released in the reaction solution in mechanism 1 (Figure 3D). Reported mechanisms for the hydrolysis of nucleic acids including RNA typically start with the catalytic action of P-diesterase enzymes such as ribonucleases to produce ribonucleotides,[51] followed by the hydrolysis of ribonucleotides into ribonucleosides and P_i by P-monoesterase enzymes including APs, as illustrated for mechanism 1 (Figure 3D).[19] In addition to mechanism 1, we investigated the three other mechanisms delineated above for the catalytic hydrolysis of RNA by our two representative plant and fungal APs (sweet potato PAP and *A. niger* phytase, respectively) (Figure 3D).

Using high-resolution LC−MS to evaluate the occurrence of the different mechanisms, we monitored the concentrations of ribonucleotides as evidence of P-diesterase activity as well as the concentrations of ribonucleosides as evidence of P-monoesterase activity (Figure 3C). We note that our data were not meant to capture the generation of small RNA fragments through possible endonuclease cleavage from the middle of the RNA chain prior to further dephosphorylation steps. Remarkably, we found a lack of increased concentrations of ribonucleotides (beyond the background residual levels) during the RNA reaction with both sweet potato PAP and *A. niger* phytase (Figure 3C). Therefore, our data did not support mechanism 1 wherein ribonucleotides would be released to the solution (Figure 3D). The *A. niger* phytase did not hydrolyze the trace amounts (∼7.8 μM) of ribonucleotides, and this finding was consistent with the low reactivity of this enzyme toward monophosphorylated ribonucleotides as reported previously.[25] In contrast, the residual concentrations of ribonucleotides (14.1 μM in plant PAP reaction) present in the crude RNA sample were hydrolyzed to ribonucleosides (∼11.9 μM) by the P-monoesterase activity of sweet potato PAP (Figure 3D). Notably, despite the absence of evolved ribonucleotides in solution, the activity of *A. niger* phytase and sweet potato PAP during the 48 h reaction resulted in the eventual accumulation of 17.4 μM and 58.2 μM ribonucleosides, respectively, thus exceeding the P-monoesterase activity of the residual ribonucleotide concentration (by nearly 16-fold and 4-fold for *A. niger* phytase and sweet potato PAP, respectively) (Figure 3D). Therefore, our data revealed P-diesterase activity coupled with the P-monoesterase activity by both enzymes, but distinguishing between mechanisms 2, 3, and 4 would require further investigation and was beyond the scope of our data (Figure 3D).

3.6. Molecular Simulations Reveal Substrate Orientation in the Active Site That Establishes Favorable Precatalytic Complex Consistent with Experimental Enzyme Kinetic Differences. The initiation of the catalytic dephosphorylation reaction requires a precatalytic enzyme−substrate complex. Here, we performed molecular docking simulations combined with molecular dynamics simulations to probe this complex for polyP or RNA bound in the substrate binding pocket of different APs, after ascertaining that our simulation protocol generated the expected precatalytic complex of reference crystal structures of *A. niger* phytase and sweet potato PAP with their reported ligands (Figure 4 and Supporting Information, Appendix G). For histidine AP enzymes like *A. niger* phytase, the precatalytic complex requires a nucleophile histidine (denoted His_{nuc}), a proton-donor aspartate (denoted Asp_{PD}), and a water molecule in close distance (<3.5 Å) to the target P-diester bond (the scissile bond)[52,53] (Figure 4C). For plant PAPs, a favorable precatalytic complex requires the coordination of the divalent cation (denoted here as M^{2+}) by the target phosphate moiety, and one water coordinated to the Fe^{3+}, likely to serve as a nucleophile water in the active site;[23,54,55] water forms a bridge between the two catalytic metals in the transition state configuration to mediate the nucleophilic attack to the P-monoester bond.[55]

For the simulated *A. niger* phytase-polyP complex, we obtained a favorable precatalytic complexation in agreement with the terminal phosphatase mechanism determined by ^{31}P NMR, whereby a terminal phosphate moiety in polyP was positioned at less than 5 Å from the two catalytic residues and from a water molecule (Figure 4A,C). Moreover, the active site residues of *A. niger* phytase participated in a total of 13 electrostatic interactions and a H-bond with the polyP chain (Figure 4A). In the complex of polyP with sweet potato PAP, beyond two electrostatic interactions between polyP and with the catalytic metals (Mn^{2+} and Fe^{3+}), there was a total of one H-bond and eight electrostatic interactions with aspartate and histidine residues (D163, H285, H322) of the active site (Figure 4B,D). Also, in agreement with the aforementioned mechanism of the polyP hydrolysis, the terminal phosphate in the polyP chain was the closest phosphate moiety (3.9 Å) to the catalytic Mn^{2+} of sweet potato PAP, and there was a water molecule in the vicinity (4 Å) of the terminal phosphate that may function as a nucleophile, albeit this water molecule was not at a favorable distance (5.5 Å) from Fe^{3+} (Figure 4B and Supporting Information, Appendix G). In sum, compared to sweet potato PAP, the molecular modeling data revealed a higher number of interactions with closer interaction distances in the catalytic center of *A. niger* phytase, thus implying a more favorable precatalytic complex with the fungal phytase than with the plant PAP, in agreement with the enzyme kinetic data for polyP dephosphorylation (Figure 4A).

By contrast to the more than ten H-bond and electrostatic interactions with polyP, there were only three interactions (1 H-bond and 2 electrostatic) formed between RNA and the active sites of *A. niger* phytase and sweet potato PAP (Figure 4). These differences in the substrate interactions in the precatalytic complexes with RNA versus polyP may underlie

https://doi.org/10.1021/acs.est.2c04948
Environ. Sci. Technol. 2022, 56, 16441−16452

the higher dephosphorylation rates of polyP than RNA determined by our enzyme kinetics experiments. In accordance, with the P-diesterase mechanism for RNA elucidated by LC−MS, our molecular simulations revealed that both enzymes interacted with a middle P-diester bond between the guanosine and the terminal adenosine of our model RNA: electrostatic interactions with two arginine residues (R62 and R58) in *A. niger* phytase and interactions with an Fe^{3+} center and a histidine residue (H324) in sweet potato PAP (Figure 4A,B). Moreover, the presence of a water molecule close to the catalytic residues (<4 Å) and the scissile P-diester bond of RNA facilitated a favorable precatalytic complex with *A. niger* phytase (Figure 4A,C). For sweet potato PAP, the presence of a water molecule between Fe^{3+} and Mn^{2+}, and in close distance (3.6 Å) to the P-diester, contributed to a potentially favorable precatalytic complex (Figure 4B,D).

The presence of the metal center has been considered as an essential requirement for the catalytic breakage of strong P-diester bonds.[56,57] For instance, the metal centers in nucleases are reported to polarize the P-diester bond, activate the nucleophile water, stabilize the transition-state, and facilitate the departure of the leaving group;[56,57] even in enzymes that use an amino acid side chain as a nucleophile, the reactivity was still improved when a metal cation was introduced.[57] As a heteronuclear metalloenzyme, sweet potato PAP presents a favorable metal center for cleaving the P-diester bonds,[58,59] which may explain our experimentally measured higher reactivity of sweet potato PAP toward RNA compared to *A. niger* phytase (Figure 2).

To expand the relevance of our theoretical findings, we performed additional molecular simulations to investigate the substrate binding mechanisms of RNA and polyP with three additional plant PAPs and three additional fungal APs (Figures 4C,D). Details on substrate interactions in the precatalytic complexes with the additional APs are provided in Supporting Information, Appendix G. Below we summarize the major findings.

The four fungal APs investigated here (*A. niger* phytase, *D. castellii* phytase, *S. cerevisiae* AP, and *K. lactis* AP) are members of the histidine AP superfamily that share a conserved catalytic site with a His_{nuc} and an Asp_{PD} as described above.[52,53,60] Consistent with the reported broad substrate specificity of *D. castellii* phytase, the polyP substrate was stabilized through the electrostatic interactions from noncatalytic residues rather than strong H-bonding to catalytic residues.[60] Previous experimental studies reported that the type 5 repressible APs like *K. lactis* AP recycled P_i from extracellular nucleotides but had negligible reactivity toward polyP chains.[61,62] Accordingly, our simulations revealed the absence of a water molecule in the active site of *K. lactis* AP to mediate the formation of the precatalytic complex with polyP, despite the interaction of polyP with the positively charged active site residues (R58 and R62 and H338) in both yeast APs (i.e., *K. lactis* AP and *S. cerevisiae* AP) (Figure 4C and Supporting Information, Appendix G). However, in the *S. cerevisiae* AP, a favorable precatalytic complex was formed due to the close distance (<4.5 Å) of a middle phosphate in polyP to the His_{nuc} and Asp_{PD} and a water molecule (Figure 4C and Supporting Information, Appendix G).

With respect to plant PAPs, we found that the number of interactions between the terminal-P moiety of polyP and the catalytic metals of the sweet potato (1 electrostatic) was less than those in thale cress PAP (2 H-bonds and 1 electrostatic) and wheat PAP (2 H-bonds) (Figure 4D and Supporting Information, Appendix G). This finding was in accordance with previous reports that sweet potato PAP exhibited a higher preference for small substrates like phosphoenolpyruvate compared to thale cress and wheat PAPs that accept bulkier substrates like phytate in their active sites.[63,64] We posit that the confined circular tunnel-shaped active site of sweet potato PAP may limit the access of the target phosphate moiety to the catalytic metals (Supporting Information, Appendix G). However, in accordance with the high preference of thale cress and wheat PAPs for P-monoester bonds,[63] the catalytic center of both enzymes oriented favorably with respect to a terminal P-monoester bond in RNA (Figure 4D and Supporting Information, Appendix G). Among the plant PAPs, similar to the polyP complex, the red kidney bean PAP participated in the most favorable interactions to complex polyP and RNA, consistent with the specificity of this enzyme for multiphosphorylated ribonucleotides:[63] there was favorable orientation of metal cations (Fe^{3+} and Zn^{2+}) with respect to a middle phosphate moiety in the polyP chain, a nearby water molecule (distance ∼2.6 Å), and the coordination of the metal catalytic center with the target phosphate moiety through 2 H-bond and 2 electrostatic interactions; the catalytic metals participated in 2 electrostatic interactions while targeting the P-diester bond in RNA (Figure 4D and Supporting Information, Appendix G). Interestingly, despite these enzyme-specific differences, our molecular simulations demonstrated that the active site residues of both plant and fungal APs engaged in a higher number of H-bonds and electrostatic interactions with polyP (5−17 interactions) compared to RNA (1−5 interactions) (Figure 4C,D). Therefore, these molecular simulation results were congruent with the experimental data on the relative dephosphorylation rates of the two P-biopolymers by the different enzymes.

3.7. Implications for P-biopolymer Dephosphorylation in Environmental Matrices. Extracellular APs are important for recycling P in environmental matrices (i.e., soils, sediments, and marine environments).[65,66] Therefore, the reactivity of these enzymes toward P-biopolymers is of special interest because P-biopolymers such as RNA and polyP are ubiquitous P sources for plant and soil microorganisms.[1−4,67] However, despite the high abundances of plant and fungal APs in P_i-deficient soils,[16] much has remained unknown about the relative reactivity kinetics and mechanisms of substrate specificity by different APs for P recycling from P-biopolymers. Here, in addition to demonstrating that our representative fungal and plant APs are both capable of dephosphorylating both polyP and RNA, we found that the extent of the reactivity toward each P-biopolymer was different for each enzyme (Figure 5). Specifically, both enzymes preferred polyP over RNA as evidenced by higher hydrolysis rates, by up to 3 orders of magnitude, with polyP than with RNA. However, the fungal phytase exhibited 10-fold higher activity for polyP hydrolysis than the plant PAP, whereas the plant PAP had 6-fold higher activity for RNA hydrolysis than the fungal phytase (Figure 5). Molecular dynamics simulations revealed up to 3-fold higher interactions in the active site of both enzymes with bound polyP compared to bound RNA, which may explain the higher rates of the enzymes toward polyP (Figure 5). Structure-based modeling of substrate-enzyme complexes was previously used to guide rational engineering of enzymes such as phytase,[68] lipase,[69,70] aminotransferase,[71] and transketolase.[72] In a similar fashion, the structural insights obtained here could contribute

https://doi.org/10.1021/acs.est.2c04948
Environ. Sci. Technol. 2022, 56, 16441−16452

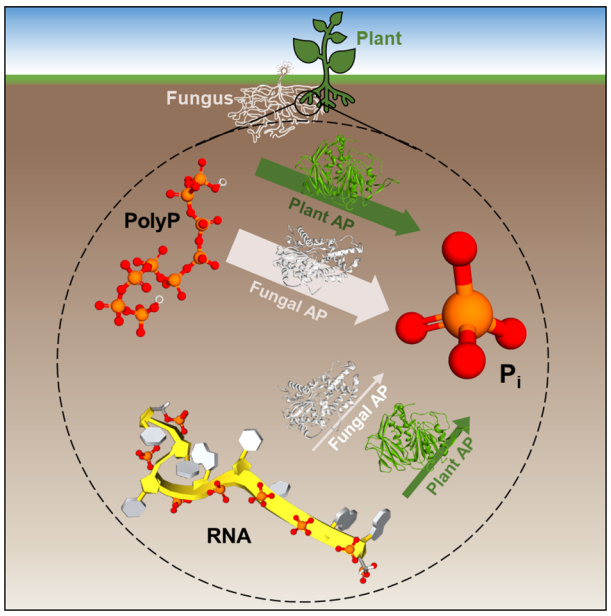

Figure 5. Schematic illustration of P-biopolymer dephosphorylation by plant and fungal acid phosphatases based on the kinetics and structural insights obtained in this study. Both fungal and plant APs preferred polyP over RNA, but fungal AP had higher reactivity toward polyP whereas plant AP was more reactive toward RNA. The arrow widths are proportional to the relative enzyme activity rates (using $\log_2$ of the relative rates). With regard to the reaction mechanisms, we determined experimentally both fungal and plant APs dephosphorylated polyP through terminal phosphatase mechanisms and dephosphorylated RNA through a coupled P-diesterase and P-monoesterase mechanism. From molecular docking simulations, the difference in each enzyme reactivity toward P-biopolymers was explained by several factors including the number of interactions, the partial charges of the substrate and active site, and the orientation of the target phosphate moiety of the substrate with respect to the catalytic center.

to guiding principles toward optimizing the activity of APs for P-polymer dephosphorylation. Using time-dependent ^{31}P NMR data, we determined that the mechanism for fast P_i extraction from polyP chains was through a sequential cleavage of the terminal phosphate moieties in the polyP chain. With regard to enzymatic reactivity toward different polyP chain lengths, the fungal phytase had the same affinity for both polyP-45 and polyP-130 but higher dephosphorylation rate for the longer-chain polyP; plant PAP had a similar rate of dephosphorylation with both polyP chain lengths. For RNA dephosphorylation mechanisms, our high-resolution LC−MS analysis determined a combined P-diesterase/P-monoesterase mechanism by both enzymes. Accordingly, the molecular modeling revealed the favorable orientation of the P-diester bond in RNA with respect to the positively charged heteronuclear metal centers of plant PAPs that can help facilitate the nucleophilic attack by an activated water molecule, thereby explaining the six times higher reactivity of the plant PAP than fungal phytase. In sum, our findings implied that the biological source of P-recycling enzymes, such as plants versus fungal communities in natural soil environments,[73] will influence the relative residence time of RNA and different sizes of polyP chains.

In organics-enriched soils, P_i bioavailability for plants and microorganisms depends on the efficiency of P_i recycling from organic P including RNA by phosphatase enzymes.[74] Our findings highlighted a one-step mechanism for the low activity of RNA dephosphorylation to generate P_i, albeit our data also pointed out inhibition of plant PAP activity at high RNA concentrations (>20 mM RNA-P). Such inhibition was likely due to steric hindrance, which has been shown to occur due to the obstruction of active sites in the presence of very high concentrations of long chain molecules.[75−77] Overcoming this inhibition by designing robust APs and related phosphatases will be necessary for P recycling purposes in complex matrices. Moreover, when both phosphorylated monomeric and polymeric substrates are present in mixtures as would be expected in the heterogeneous soil organic matter content, the kinetics of P-biopolymer dephosphorylation by phosphatases may be different from our results. A previous study reported that the dephosphorylation kinetics of ribonucleotide monomers by *A. niger* phytase was negatively affected by competition from other small phosphorylated organic substrates.[24] The extent of similar competition for the dephosphorylation of P-biopolymers remains to be investigated.

The polyP-accumulating organisms (PAOs), which are especially more abundant in rhizosphere than bulk soil,[67] have been employed to engineer enhanced biological P removal (EBPR) in wastewater treatment plants to store P_i in the form of polyP chains.[78] Relevant to the subsequent application of polyP-containing biosolids from EBPR processed as fertilizers in agricultural soils,[78] our data stressed the higher rate of fungal phytase than plant PAP to dephosphorylate polyP and, importantly, that the fungal phytase was not inhibited in the presence of high concentrations of P_i (>0.3 mM) or polyP chains (>20 μM polyP chains). Such favorable reactivity of fungal phytase toward polyP should also be considered in interpretating P recycling in environments, such as wetland soils with high polyP concentration.[67,79]

Acknowledging the potential adsorption of phosphatase enzymes and P-biopolymers to soil minerals and marine sediments,[26,74,80−82] we anticipate that the dephosphorylation rates reported here would be modulated in the natural soil environment depending on soil pH conditions, soil mineral types, and soil organic composition. Compared to heterogeneous oxisol clays, it was reported that there was up to 70% more decrease in the phytate dephosphorylation rate by *A. niger* phytase in suspensions with pure soil minerals such as goethite, hematite, kaolinite, and montmorillonite.[83] Furthermore, an alkaline phosphatase from *E. coli* was reported to undergo near-complete activity loss when adsorbed to marine sediments, but about 30% of activity still remained when adsorbed to soil minerals including goethite and montmorillonite.[84] However, when a soil suspension was precoated with adsorbed protein, there was a decrease in phytase adsorption.[26] Therefore, these previous studies implied that the extent of inhibition of the activity of each enzyme in the soil matrix will depend on the soil mineral and organic compositions. Relevant to the new findings presented here, it remains to be elucidated to which extent adsorption to the heterogeneous matrix of soils and sediments would modulate the catalytic activity and conformational stability of different phosphatases in relation to P recycling from P-biopolymers.

■ ASSOCIATED CONTENT

Supporting Information

The Supporting Information is available free of charge at https://pubs.acs.org/doi/10.1021/acs.est.2c04948.

https://doi.org/10.1021/acs.est.2c04948
Environ. Sci. Technol. 2022, 56, 16441−16452

Supporting text, figures, and tables for this study as referred to in the main text, including details on materials, the RNA characterization procedure, enzyme preparation procedures, measurement of oxygen isotope values, and time-dependent changes in the ^{31}P NMR peak intensities, kinetics profiles of polyP and RNA dephosphorylation by *A. niger* phytase and sweet potato PAP, and molecular dynamics simulations (PDF)

AUTHOR INFORMATION

Corresponding Author

Ludmilla Aristilde − *Department of Biological and Environmental Engineering, College of Agriculture and Life Sciences, Cornell University, Ithaca, New York 14853, United States; Department of Civil and Environmental Engineering, McCormick School of Engineering and Applied Science, Northwestern University, Evanston, Illinois 60208, United States;* orcid.org/0000-0002-8566-1486; Phone: 847-491-2999; Email: ludmilla.aristilde@northwestern.edu

Authors

Mina Solhtalab − *Department of Biological and Environmental Engineering, College of Agriculture and Life Sciences, Cornell University, Ithaca, New York 14853, United States; Department of Civil and Environmental Engineering, McCormick School of Engineering and Applied Science, Northwestern University, Evanston, Illinois 60208, United States*

Spencer R. Moller − *Department of Plant and Soil Sciences, University of Delaware, Newark, Delaware 19716, United States;* orcid.org/0000-0003-1423-0563

April Z. Gu − *School of Civil and Environmental Engineering, College of Engineering, Cornell University, Ithaca, New York 14853, United States;* orcid.org/0000-0002-5099-5531

Deb Jaisi − *Department of Plant and Soil Sciences, University of Delaware, Newark, Delaware 19716, United States;* orcid.org/0000-0001-8934-3832

Complete contact information is available at: https://pubs.acs.org/10.1021/acs.est.2c04948

Notes

The authors declare no competing financial interest.

ACKNOWLEDGMENTS

Funding for this research and for the Ph.D. studies of M.S. was provided by a collaborative research grant awarded to L.A. and D.J. from the U.S. National Science Foundation (NSF CHE-1709626). This work made use of the IMSERC NMR spectroscopy facility and NUseq core at Northwestern University. We would like to thank Danielle Tullman-Ercek and Carolyn Mills for providing the facilities for purification of *A. niger* phytase used in this study. Thanks to Neal Blair for providing us a SpeedVac Vacuum Concentrator for concentrating our hydrolyzed RNA samples.

REFERENCES

(1) Dell'Anno, A.; Danovaro, R. Extracellular DNA plays a key role in deep-sea ecosystem functioning. *Science* **2005**, *309* (5744), 2179−2179.

(2) Schulz-Vogt, H. N.; Pollehne, F.; Jurgens, K.; Arz, H. W.; Beier, S.; Bahlo, R.; Dellwig, O.; Henkel, J. V.; Herlemann, D. P. R.; Kruger, S.; Leipe, T.; Schott, T. Effect of large magnetotactic bacteria with polyphosphate inclusions on the phosphate profile of the suboxic zone in the Black Sea. *ISME journal* **2019**, *13* (5), 1198−1208.

(3) Yamaguchi, T.; Sato, M.; Hashihama, F.; Ehama, M.; Shiozaki, T.; Takahashi, K.; Furuya, K. Basin-scale variations in labile dissolved phosphoric monoesters and diesters in the central North Pacific Ocean. *Journal of Geophysical Research: Oceans* **2019**, *124* (5), 3058−3072.

(4) Ma, H.; Zhu, Y.; Jiang, J.; Bing, X.; Xu, W.; Hu, X.; Zhang, S.; Shen, Y.; He, Z. Characteristics of inorganic and organic phosphorus in Lake Sha sediments from a semiarid region, Northwest China: Sources and bioavailability. *Appl. Geochem.* **2022**, *137*, 105209.

(5) Wang, L.; Amelung, W.; Prietzel, J.; Willbold, S. Transformation of organic phosphorus compounds during 1500 years of organic soil formation in Bavarian Alpine forests−A 31P NMR study. *Geoderma* **2019**, *340*, 192−205.

(6) Hurt, R. A.; Qiu, X.; Wu, L.; Roh, Y.; Palumbo, A. V.; Tiedje, J. M.; Zhou, J. Simultaneous recovery of RNA and DNA from soils and sediments. *Appl. Environ. Microbiol.* **2001**, *67* (10), 4495−4503.

(7) Perillo, V. L.; Cade-Menun, B. J.; Ivancic, M.; Ross, D. S.; Wemple, B. C. Land use and landscape position influence soil organic phosphorus speciation in a mixed land use watershed. *J. Environ. Qual.* **2021**, *50* (4), 967−978.

(8) Wang, X.; Gao, Y.; Chu, G. Optimization and Characterization of Polyphosphate Fertilizers by Two Different Manufacturing Processes. *ACS omega* **2021**, *6* (29), 18811−18822.

(9) Omelon, S. J.; Grynpas, M. D. Relationships between polyphosphate chemistry, biochemistry and apatite biomineralization. *Chem. Rev.* **2008**, *108* (11), 4694−4715.

(10) Yang, W. Nucleases: diversity of structure, function and mechanism. *Q. Rev. Biophys.* **2011**, *44* (1), 1−93.

(11) Albi, T.; Serrano, A. Inorganic Polyphosphate in the Microbial World. Emerging Roles for a Multifaceted Biopolymer. *World J. Microbiol. Biotechnol.* **2016**, *32* (2), 1−12.

(12) Liang, Y.; Blake, R. E. Compound-and enzyme-specific phosphodiester hydrolysis mechanisms revealed by δ18O of dissolved inorganic phosphate: Implications for marine P cycling. *Geochim. Cosmochim. Acta* **2009**, *73* (13), 3782−3794.

(13) Jarosch, K. A.; Kandeler, E.; Frossard, E.; Bünemann, E. K. Is the enzymatic hydrolysis of soil organic phosphorus compounds limited by enzyme or substrate availability? *Soil Biology and Biochemistry* **2019**, *139*, 107628.

(14) Lee, S. F.; Davey, L. Disulfide bonds: a key modification in bacterial extracytoplasmic proteins. *Journal of Dental Research* **2017**, *96* (13), 1465−1473.

(15) Forrest, S.; Welch, M. Arming the troops: Post-translational modification of extracellular bacterial proteins. *Science Progress* **2020**, *103* (4), 1.

(16) Yao, Q.; Li, Z.; Song, Y.; Wright, S. J.; Guo, X.; Tringe, S. G.; Tfaily, M. M.; Pasa-Tolic, L.; Hazen, T. C.; Turner, B. L.; Mayes, M. A.; Pan, C. Community proteogenomics reveals the systemic impact of phosphorus availability on microbial functions in tropical soil. *Nature ecology & evolution* **2018**, *2* (3), 499−509.

(17) Ezawa, T.; Hayatsu, M.; Saito, M. A new hypothesis on the strategy for acquisition of phosphorus in arbuscular mycorrhiza: up-regulation of secreted acid phosphatase gene in the host plant. *Mol. Plant-Microbe Interact.* **2005**, *18* (10), 1046−1053.

(18) Wang, L.; Li, Z.; Qian, W.; Guo, W.; Gao, X.; Huang, L.; Wang, H.; Zhu, H.; Wu, J.-W.; Wang, D.; Liu, D. The Arabidopsis purple acid phosphatase AtPAP10 is predominantly associated with the root surface and plays an important role in plant tolerance to phosphate limitation. *Plant Physiology* **2011**, *157* (3), 1283−1299.

(19) Gaind, S.; Nain, L. Soil−phosphorus mobilization potential of phytate mineralizing fungi. *Journal of plant nutrition* **2015**, *38* (14), 2159−2175.

(20) Margalef, O.; Sardans, J.; Fernandez-Martinez, M.; Molowny-Horas, R.; Janssens, I. A.; Ciais, P.; Goll, D.; Richter, A.; Obersteiner, M.; Asensio, D.; Penuelas, J. Global patterns of phosphatase activity in natural soils. *Sci. Rep.* **2017**, *7* (1), 1−13.

(21) Ma, X.; Li, H.; Zhang, J.; Shen, J. Spatiotemporal Pattern of Acid Phosphatase Activity in Soils Cultivated With Maize Sensing to Phosphorus-Rich Patches. *Frontiers in plant science* **2021**, *12*, 650436.
(22) Yadav, R. S.; Tarafdar, J. C. Phytase and phosphatase producing fungi in arid and semi-arid soils and their efficiency in hydrolyzing different organic P compounds. *Soil Biology and Biochemistry* **2003**, *35* (6), 745−751.
(23) Schenk, G.; Mitić, N.; Hanson, G. R.; Comba, P. Purple acid phosphatase: a journey into the function and mechanism of a colorful enzyme. *Coord. Chem. Rev.* **2013**, *257* (2), 473−482.
(24) Mullaney, E. J.; Ullah, A. H. The term phytase comprises several different classes of enzymes. *Biochemical and biophysical research communications* **2003**, *312* (1), 179−184.
(25) Solhtalab, M.; Klein, A. R.; Aristilde, L. Hierarchical reactivity of enzyme-mediated phosphorus recycling from organic mixtures by Aspergillus niger phytase. *J. Agric. Food Chem.* **2021**, *69* (7), 2295−2305.
(26) George, T. S.; Simpson, R. J.; Gregory, P. J.; Richardson, A. E. Differential interaction of Aspergillus niger and Peniophora lycii phytases with soil particles affects the hydrolysis of inositol phosphates. *Soil Biology and Biochemistry* **2007**, *39* (3), 793−803.
(27) Lei, X. G.; Weaver, J. D.; Mullaney, E.; Ullah, A. H.; Azain, M. J. Phytase, a new life for an "old" enzyme. *Annu. Rev. Anim. Biosci.* **2013**, *1* (1), 283−309.
(28) Huang, R.; Wan, B.; Hultz, M.; Diaz, J. M.; Tang, Y. Phosphatase-mediated hydrolysis of linear polyphosphates. *Environ. Sci. Technol.* **2018**, *52* (3), 1183−1190.
(29) Bai, Y.; Stout, L.; Unal-Tosun, G.; Li, J.; Jaisi, D. Synthesis and Degradation of Polyphosphate: Isotope Effects in Enzyme-and Bacteria-Catalyzed Reactions. *ACS Earth and Space Chemistry* **2020**, *4* (12), 2327−2336.
(30) Park, Y.; Malliakas, C. D.; Zhou, Q.; Gu, A. Z.; Aristilde, L. Molecular Coordination, Structure, and Stability of Metal-Polyphosphate Complexes Resolved by Molecular Modeling and X-ray Scattering: Structural Insights on the Biological Fate of Polyphosphate. *Environ. Sci. Technol.* **2021**, *55* (20), 14185−14193.
(31) Schenk, G.; Mitić, N.; Hanson, G. R.; Comba, P. Purple acid phosphatase: a journey into the function and mechanism of a colorful enzyme. *Coord. Chem. Rev.* **2013**, *257* (2), 473−482.
(32) Jaisi, D. P.; Blake, R. E. Tracing sources and cycling of phosphorus in Peru Margin sediments using oxygen isotopes in authigenic and detrital phosphates. *Geochim. Cosmochim. Acta* **2010**, *74*, 3199−3212.
(33) Jaisi, D. P.; Blake, R. E. Advances in using oxygen isotope ratios of phosphate to understand phosphorus cycling in the environment, *Advances in Agronomy*; Elsevier, 2014; pp 1−53.
(34) Clesceri, L.; Greensberg, A.; Eaton, A. Standard Methods for the Examination of Water and Wastewater, 51st ed.; *Am. J. Public Health*; Clesceri, L., Greensberg, A., Eaton, A., Eds.; Washington, DC, 1999.
(35) Liu, X.; Ser, Z.; Locasale, J. W. Development and quantitative evaluation of a high-resolution metabolomics technology. *Analytical chemistry* **2014**, *86* (4), 2175−2184.
(36) Benkert, P.; Tosatto, S. C.; Schomburg, D. QMEAN: A comprehensive scoring function for model quality assessment. *Proteins: Struct., Funct., Bioinf.* **2008**, *71* (1), 261−277.
(37) Accelry's. *Discovery Studio Modeling Environment*; Accelrys Software Inc.: San Diego, 2013.
(38) Parnell, A. E.; Mordhorst, S.; Kemper, F.; Giurrandino, M.; Prince, J. P.; Schwarzer, N. J.; Hofer, A.; Wohlwend, D.; Jessen, H. J.; Gerhardt, S.; Einsle, O.; Oyston, P. C. F.; Andexer, J. N.; Roach, P. L. Substrate recognition and mechanism revealed by ligand-bound polyphosphate kinase 2 structures. *Proc. Natl. Acad. Sci. U. S. A.* **2018**, *115* (13), 3350−3355.
(39) Yan, Y.; Tao, H.; He, J.; Huang, S. Y. The HDOCK server for integrated protein−protein docking. *Nature protocols* **2020**, *15* (5), 1829−1852.
(40) Tamburini, F.; Pfahler, V.; von Sperber, C.; Frossard, E.; Bernasconi, S. M. Oxygen isotopes for unraveling phosphorus transformations in the soil−plant system: A review. *Soil Science Society of America Journal* **2014**, *78* (1), 38−46.
(41) von Sperber, C.; Tamburini, F.; Brunner, B.; Bernasconi, S. M.; Frossard, E. The oxygen isotope composition of phosphate released from phytic acid by the activity of wheat and Aspergillus niger phytase. *Biogeosciences* **2015**, *12*, 4175−4184.
(42) Helfenstein, J.; Tamburini, F.; von Sperber, C.; Massey, M. S.; Pistocchi, C.; Chadwick, O. A.; Vitousek, P. M.; Kretzschmar, R.; Frossard, E. Combining spectroscopic and isotopic techniques gives a dynamic view of phosphorus cycling in soil. *Nat. Commun.* **2018**, *9* (1), 1−9.
(43) Stout, L. M.; Joshi, S. R.; Kana, T. M.; Jaisi, D. P. Microbial activities and phosphorus cycling: An application of oxygen isotope ratios in phosphate. *Geochim. Cosmochim. Acta* **2014**, *138*, 101−116.
(44) Sun, M.; Alikhani, J.; Massoudieh, A.; Greiner, R.; Jaisi, D. P. Phytate degradation by different phosphohydrolase enzymes: contrasting kinetics, decay rates, pathways, and isotope effects. *Soil Science Society of America Journal* **2017**, *81*, 61−75.
(45) Kendall, C. Tracing nitrogen sources and cycling in catchments. In *Isotope tracers in catchment hydrology*; Elsevier, 1998; pp 519−576.
(46) Wu, L.; Yao, J.; Trebse, P.; Zhang, N.; Richnow, H. H. Compound specific isotope analysis of organophosphorus pesticides. *Chemosphere* **2014**, *111*, 458−463.
(47) Jammer, S.; Voloshenko, A.; Gelman, F.; Lev, O. Chiral and isotope analyses for assessing the degradation of organic contaminants in the environment: Rayleigh dependence. *Environ. Sci. Technol.* **2014**, *48* (6), 3310−3318.
(48) Hirschorn, S. K.; Dinglasan, M. J.; Elsner, M.; Mancini, S. A.; Lacrampe-Couloume, G.; Edwards, E. A.; Sherwood Lollar, B. Pathway dependent isotopic fractionation during aerobic biodegradation of 1, 2-dichloroethane. *Environ. Sci. Technol.* **2004**, *38* (18), 4775−4781.
(49) Elsner, M. Stable isotope fractionation to investigate natural transformation mechanisms of organic contaminants: principles, prospects and limitations. *Journal of Environmental Monitoring* **2010**, *12* (11), 2005−2031.
(50) de Oliveira Lima, E. C.; Moita Neto, J. M.; Fujiwara, F. Y.; Galembeck, F. Aluminum polyphosphate thermoreversible gels: A study by 31P and 27Al NMR spectroscopy. *J. Colloid Interface Sci.* **1995**, *176* (2), 388−396.
(51) Cassano, A. G.; Anderson, V. E.; Harris, M. E. Understanding the transition states of phosphodiester bond cleavage: insights from heavy atom isotope effects. *Biopolymers: Original Research on Biomolecules* **2004**, *73* (1), 110−129.
(52) Rigden, D. J. The histidine phosphatase superfamily: structure and function. *Biochem. J.* **2008**, *409* (2), 333−348.
(53) Oakley, A. J. The structure of Aspergillus niger phytase PhyA in complex with a phytate mimetic. *Biochem. Biophys. Res. Commun.* **2010**, *397* (4), 745−749.
(54) Retegan, M.; Milet, A.; Jamet, H. Comparative theoretical studies of the phosphomonoester hydrolysis mechanism by purple acid phosphatases. *J. Phys. Chem. A* **2010**, *114* (26), 7110−7116.
(55) Zhou, X.; Zhang, X. P.; Li, W.; Phillips, D. L.; Ke, Z.; Zhao, C. Electronic Effect on Bimetallic Catalysts: Cleavage of Phosphodiester Mediated by Fe (III)−Zn (II) Purple Acid Phosphatase Mimics. *Inorg. Chem.* **2020**, *59* (17), 12065−12074.
(56) Dupureur, C. M. Roles of metal ions in nucleases. *Curr. Opin. Chem. Biol.* **2008**, *12* (2), 250−255.
(57) Dupureur, C. M. One is enough: insights into the two-metal ion nuclease mechanism from global analysis and computational studies. *Metallomics* **2010**, *2* (9), 609−620.
(58) Verge, F.; Lebrun, C.; Fontecave, M.; Ménage, S. Hydrolysis of phosphodiesters by diiron complexes: design of nonequivalent iron sites in purple acid phosphatase models. *Inorganic chemistry* **2003**, *42* (2), 499−507.
(59) Lanznaster, M.; Neves, A.; Bortoluzzi, A. J.; Aires, V. V. E.; Szpoganicz, B.; Terenzi, H.; Severino, P. C.; Fuller, J. M.; Drew, S. C.; Gahan, L. R.; Hanson, G. R.; Riley, M. J.; Schenk, G. A new heterobinuclear FeIIICuII complex with a single terminal FeIII−O

(phenolate) bond. Relevance to purple acid phosphatases and nucleases. *JBIC Journal of Biological Inorganic Chemistry* **2005**, *10* (4), 319−332.
(60) Ragon, M.; Hoh, F.; Aumelas, A.; Chiche, L.; Moulin, G.; Boze, H. Structure of Debaryomyces castellii CBS 2923 phytase. *Acta Crystallographica Section F: Structural Biology and Crystallization Communications* **2009**, *65* (4), 321−326.
(61) Kennedy, E. J.; Pillus, L.; Ghosh, G. Pho5p and newly identified nucleotide pyrophosphatases/phosphodiesterases regulate extracellular nucleotide phosphate metabolism in Saccharomyces cerevisiae. *Eukaryotic Cell* **2005**, *4* (11), 1892−1901.
(62) Andreeva, N.; Ledova, L.; Ryasanova, L.; Kulakovskaya, T.; Eldarov, M. The acid phosphatase Pho5 of Saccharomyces cerevisiae is not involved in polyphosphate breakdown. *Folia microbiologica* **2019**, *64* (6), 867−873.
(63) Feder, D.; McGeary, R. P.; Mitic, N.; Lonhienne, T.; Furtado, A.; Schulz, B. L.; Henry, R. J.; Schmidt, S.; Guddat, L. W.; Schenk, G. Structural elements that modulate the substrate specificity of plant purple acid phosphatases: avenues for improved phosphorus acquisition in crops. *Plant Science* **2020**, *294*, 110445.
(64) Faba-Rodriguez, R.; Gu, Y.; Salmon, M.; Dionisio, G.; Brinch-Pedersen, H.; Brearley, C. A.; Hemmings, A. M. Structure of a cereal purple acid phytase provides new insights to phytate degradation in plants. *Plant communications* **2022**, *3* (2), 100305.
(65) Burns, R. G., Dick, R. P. *Enzymes in the environment: activity, ecology, and applications*; CRC Press, 2002.
(66) Duhamel, S.; Diaz, J. M.; Adams, J. C.; Djaoudi, K.; Steck, V.; Waggoner, E. M. Phosphorus as an integral component of global marine biogeochemistry. *Nature Geoscience* **2021**, *14*, 359−368.
(67) Akbari, A.; Wang, Z.; He, P.; Wang, D.; Lee, J.; Han, I.; Li, G.; Gu, A. Z. Unrevealed roles of polyphosphate-accumulating microorganisms. *Microbial Biotechnology* **2021**, *14* (1), 82−87.
(68) Fakhravar, A.; Hesampour, A. Rational design-based engineering of a thermostable phytase by site-directed mutagenesis. *Molecular biology reports* **2018**, *45* (6), 2053−2061.
(69) Dror, A.; Shemesh, E.; Dayan, N.; Fishman, A. Protein engineering by random mutagenesis and structure-guided consensus of *Geobacillus stearothermophilus* lipase T6 for enhanced stability in methanol. *Applied and environmental microbiology* **2014**, *80* (4), 1515−1527.
(70) Ebert, M. C.; Pelletier, J. N. Computational tools for enzyme improvement: why everyone can−and should−use them. *Curr. Opin. Chem. Biol.* **2017**, *37*, 89−96.
(71) Sirin, S.; Kumar, R.; Martinez, C.; Karmilowicz, M. J.; Ghosh, P.; Abramov, Y. A.; Martin, V.; Sherman, W. A computational approach to enzyme design: predicting ω-aminotransferase catalytic activity using docking and MM-GBSA scoring. *J. Chem. Inf. Model.* **2014**, *54* (8), 2334−2346.
(72) Payongsri, P.; Steadman, D.; Strafford, J.; MacMurray, A.; Hailes, H. C.; Dalby, P. A. Rational substrate and enzyme engineering of transketolase for aromatics. *Organic & biomolecular chemistry* **2012**, *10* (45), 9021−9029.
(73) Toju, H.; Sato, H.; Yamamoto, S.; Kadowaki, K.; Tanabe, A. S.; Yazawa, S.; Nishimura, O.; Agata, K. How are plant and fungal communities linked to each other in belowground ecosystems? A massively parallel pyrosequencing analysis of the association specificity of root-associated fungi and their host plants. *Ecology and evolution* **2013**, *3* (9), 3112−3124.
(74) Burns, R. G.; DeForest, J. L.; Marxsen, J.; Sinsabaugh, R. L.; Stromberger, M. E.; Wallenstein, M. D.; Weintraub, M. N.; Zoppini, A. Soil enzymes in a changing environment: current knowledge and future directions. *Soil Biology and Biochemistry* **2013**, *58*, 216−234.
(75) Ventura, S. P.; Santos, L. D.; Saraiva, J. A.; Coutinho, J. A. Concentration effect of hydrophilic ionic liquids on the enzymatic activity of Candida antarctica lipase B. *World J. Microbiol. Biotechnol.* **2012**, *28* (6), 2303−2310.
(76) Solhtalab, M.; Karbalaei-Heidari, H. R.; Absalan, G. Tuning of hydrophilic ionic liquids concentration: A way to prevent enzyme instability. *Journal of Molecular Catalysis B: Enzymatic* **2015**, *122*, 125−130.
(77) Cha, H. J.; Park, J. B.; Park, S. Esterification of secondary alcohols and multi-hydroxyl compounds by Candida antarctica lipase B and subtilisin. *Biotechnology and Bioprocess Engineering* **2019**, *24* (1), 41−47.
(78) Saia, S. M.; Carrick, H. J.; Buda, A. R.; Regan, J. M.; Walter, M. T. Critical Review of Polyphosphate and Polyphosphate Accumulating Organisms for Agricultural Water Quality Management. *Environ. Sci. Technol.* **2021**, *55* (5), 2722−2742.
(79) Cheesman, A. W.; Turner, B. L.; Reddy, K. R. Forms of organic phosphorus in wetland soils. *Biogeosciences* **2014**, *11* (23), 6697−6710.
(80) Bachman, P.; Fischer, J.; Song, Z.; Urbanczyk-Wochniak, E.; Watson, G. Environmental fate and dissipation of applied dsRNA in soil, aquatic systems, and plants. *Frontiers in Plant Science* **2020**, *11*, 21.
(81) Wan, B.; Elzinga, E. J.; Huang, R.; Tang, Y. Molecular mechanism of linear polyphosphate adsorption on iron and aluminum oxides. *J. Phys. Chem. C* **2020**, *124* (52), 28448−28457.
(82) Wan, B.; Huang, R.; Diaz, J. M.; Tang, Y. Rethinking the biotic and abiotic remineralization of complex phosphate molecules in soils and sediments. *Science of The Total Environment* **2022**, *833*, 155187.
(83) Giaveno, C.; Celi, L.; Richardson, A. E.; Simpson, R. J.; Barberis, E. Interaction of phytases with minerals and availability of substrate affect the hydrolysis of inositol phosphates. *Soil Biology and Biochemistry* **2010**, *42* (3), 491−498.
(84) Zhu, Y.; Wu, F.; Feng, W.; Liu, S.; Giesy, J. P. Interaction of alkaline phosphatase with minerals and sediments: activities, kinetics and hydrolysis of organic phosphorus. *Colloids Surf., A* **2016**, *495*, 46−53.

https://doi.org/10.1021/acs.est.2c04948
Environ. Sci. Technol. 2022, 56, 16441−16452